Monthly Notices
of the
ROYAL ASTRONOMICAL SOCIETY

MNRAS **493,** 2207–2214 (2020)
Advance Access publication 2020 January 3

doi:10.1093/mnras/stz3634

TOROS optical follow-up of the advanced LIGO–VIRGO O2 second observational campaign

Rodolfo Artola,[1] Martin Beroiz,[2] Juan Cabral,[1] Richard Camuccio,[2] Moises Castillo,[2] Vahram Chavushyan,[3] Carlos Colazo,[1] Hector Cuevas,[4] Darren L. DePoy,[5] Mario C. Díaz,[2] Mariano Domínguez,[1] Deborah Dultzin,[6] Daniela Fernández,[7] Antonio C. Ferreyra,[1] Aldo Fonrouge,[2] José Franco,[6] Darío Graña,[1] Carla Girardini,[1] Sebastián Gurovich,[1] Antonio Kanaan,[8] Diego G. Lambas,[1] Marcelo Lares,[1] Alejandro F. Hinojosa,[2] Andrea Hinojosa,[2] Americo F. Hinojosa,[2] Omar López-Cruz,[3] Lucas M. Macri,[5] Jennifer L. Marshall,[5] Raul Melia,[1] Wendy Mendoza,[2] José L. Nilo Castellón,[4,9] Nelson Padilla,[7] Victor Perez,[2] Tania Peñuela,[2] Wahltyn Rattray,[2] Víctor Renzi,[1] Emmanuel Ríos-López,[3] Amelia Ramírez Rivera,[4] Tiago Ribeiro,[10] Horacio Rodriguez,[1] Bruno Sánchez,[11] Matías Schneiter,[1] William Schoenell,[12] Manuel Starck,[1] Rubén Vrech,[1] Cecilia Quiñones,[1] Luis Tapia,[1] Marina Tornatore,[1] Sergio Torres-Flores,[4] Ervin Vilchis[2] and Adam Zadrożny[2,13]★

Affiliations are listed at the end of the paper

Accepted 2019 December 20. Received 2019 December 19; in original form 2019 June 25

ABSTRACT

We present the methods and results of the optical follow-up, conducted by the Transient Optical Robotic Observatory of the South Collaboration, of gravitational wave events detected during the Advanced LIGO–Virgo second observing run (2016 November–2017 August). Given the limited field of view (∼100 arcmin) of our observational instrumentation, we targeted galaxies within the area of high localization probability that were observable from our sites. We analysed the observations using difference imaging, followed by a random forest algorithm to discriminate between real and spurious transients. Our observations were conducted using telescopes at Estación Astrofísica de Bosque Alegre, Cerro Tololo Inter-American Observatory, the Dr. Cristina V. Torres Memorial Astronomical Observatory, and an observing station in Salta, Argentina.

Key words: gravitational waves – methods: data analysis – telescopes.

1 INTRODUCTION

The network of advanced ground-based gravitational wave (GW) interferometers consisting of the LIGO observatories (LIGO Scientific Collaboration 2015) and the VIRGO observatory (Acernese et al. 2015) conducted their second observing run (O2) between 2016 November and 2017 August. The detectors are designed to be capable of detecting GWs emitted by the mergers of compact objects in systems like binary neutron stars (BNSs), binary black holes (BBHs), or black hole–neutron star (BHNS) systems, out to distances of hundreds of Mpc (see Abbott et al. 2016a, and references therein).

It is expected that if the mergers of compact objects contain at least one neutron star, electromagnetic (EM) radiation will be emitted during the event. Different EM counterparts, arising from expanding r-process ejecta and from the interaction with the surrounding stellar environment, could range from very short duration gamma-ray bursts (GRBs) and X-rays to longer duration emission at optical, near-infrared, and radio wavelengths (Li & Paczyński 1998; Nakar & Piran 2011; Metzger & Berger 2012; Barnes & Kasen 2013; Berger 2014; Cowperthwaite & Berger 2015). The simultaneous detection of a merger event by GW and EM observatories provides an integrated astrophysical interpretation of the event and is instrumental in producing better estimates for the

★ E-mail: Adam.Zadrozny@ncbj.gov.pl

distance and energy scales of the event as well as improving the estimation of its orbital parameters.

The 'Transient Optical Robotic Observatory of the South' (TOROS; Benacquista et al. 2014) Collaboration was formed, motivated by the desire to participate in the observations of EM counterparts to GW events. TOROS seeks to ultimately deploy a wide-field optical telescope on Cordón Macón in the Atacama Plateau of Northwestern Argentina (Renzi et al. 2009; Tremblin et al. 2012). Independently of the pursuit of this goal, the collaboration had access to other astronomical resources that we will describe in Section 2.2.

TOROS participated in the second observing run O2, under a memorandum of understanding (MOU) with the LIGO/VIRGO collaboration (LVC) from 2016 November to 2017 August. Under the same MOU, we also participated in the previous observing run O1, from 2015 September to 2016 January.

The GW events detected during the O1 and O2 science runs are described in GWTC-1: a GW transient catalogue of compact binary mergers (LIGO Scientific Collaboration & Virgo Collaboration 2018) published by the LIGO and Virgo Scientific Collaboration. Up until 2018 November 30, there were 11 GW events known. Ten of them were identified as BBH mergers and one, GW170817, as a BNS merger.

This paper is organized as follows: Section 2 discusses our observations and instruments; Section 3 describes the data reduction method, difference imaging algorithms, and the classification of bogus and real transients; Section 4 presents our results; Section 5 describes future plans for TOROS; Section 6 summarizes our findings.

2 OBSERVATIONS

2.1 Alerts

During the O2 science run, the TOROS network responded to three alerts: G268556 (LSC & Virgo 2017a), G270580 (LSC & Virgo 2017b), and G298048 (LSC & Virgo 2017c). Candidate G268556 was later confirmed as astrophysical and promoted to GW170104, as well as G298048, which became GW170817. Alert G270580 was later determined to be non-astrophysical and retracted.

GW170104 was followed up by Estación Astrofísica de Bosque Alegre (EABA) and it was imaged 9–11 d after the event. G270580 was followed by EABA, but the quality of the images obtained was too poor to allow for a useful analysis. GW170817 was followed up by the EABA and T80-South (T80S) facilities. For this last case, we observed targets generated from our broker system and we also observed the optical counterpart reported by the 1M2H Collaboration (Abbott et al. 2017; Díaz et al. 2017).

2.2 Instruments

Over the period of O2, TOROS had access to instruments in four facilities, namely

(i) A 1.5-m telescope at the EABA in Argentina with an unfiltered CCD.

(ii) The 0.826-m T80S at the Cerro Tololo Inter-American Observatory in Chile, with a 2 deg^2 field of view and *g*, *r*, and *i* Sloan filters.

(iii) The 0.4-m telescope at the Dr. Cristina V. Torres Memorial Astronomical Observatory (CTMO) in Texas, USA, with an unfiltered CCD.

(iv) A 16-in. Meade LX200 telescope, with unfiltered SBIG STF 8300 camera, and a field of view of 15.3 arcmin × 11.5 arcmin, in Salta, Argentina.

Additionally, during the 2017A semester, TOROS had access to the Gran Telescopio Canarias (GTC), a segmented 10-m telescope located at La Palma in the Canary Islands. TOROS was assigned 5 h of target of opportunity by the Mexican Time Allocation Committee (TAC). The Mexican chapter of TOROS had access to the 2.1-m telescope at the Guillermo Haro Observatory (OAGH) in Cananea Sonora as well.

3 METHOD

In this section, we discuss the standard response method to GW alerts during O2 and the subsequent image processing.

3.1 Telescope pointing strategy

The first step when processing an alert is the selection of targets to observe. To search for EM counterparts, we use a galaxy-based approach. For each potential GW event detected, LIGO–Virgo issues a position probability map for the origin of the event. Even for 90 per cent confidence regions, the probability map usually covers a large area, typically larger than 100 deg^2 For small FoV telescopes, like the ∼0.5 deg^2 FoV telescopes available to TOROS during O2, it is not practical to scan the whole high-probability localization area.

Instead, we assume a compromise between pre-selection biases and viable increase in recovery rate, and also between additional time for new pointing and the short time-scale of the transient events associated with GWs. For this reason, we decided to target only massive galaxies in the highest probability sky regions. This is not too much of a limitation though, since the probability of occurrence of NS or BH mergers is higher in close proximity to galaxies with considerable mass. In fact, Hanna, Mandel & Vousden (2014) showed that the use of galaxy catalogues can improve success rates by 10 per cent and up to three times compared to not utilizing these kinds of catalogues. The discovery of the first joint GW–EM emission in close proximity to NGC 4993 corroborates the validity of this approach.

In implementing this strategy, we compare the probability map for the origin of the GW event against objects in the Gravitational Wave Galaxy Catalogue (GWGC; White, Daw & Dhillon 2011) and we choose the top 20 galaxies, ranking them by their probability to be connected to the event. We also used additional cuts on the parameters for observability of the target galaxies, and their position above the horizon.

In particular, the impact of one of those parameters – a too conservative cut in RA for observability – caused object NGC 4993 to fall outside the target list for the GW170817 event. We discuss this incident, its implications, and attempts to remedy this, in more detail, in Section 4.3.1.

3.2 Image pre-processing

The initial data reduction followed the standard procedure for bias and dark subtraction, flat-fielding using twilight sky frames, and illumination correction.

The astrometry was solved using the ASTROMETRY.NET program (Lang et al. 2010). The extraction of sources from the images is done in most cases with the software SEXTRACTOR (Bertin & Arnouts 1996) unless specified otherwise.

Table 1. SEXTRACTOR parameters for Machine Learning.

ID	Parameter
1, 2	FLUX_APER, FLUXERR_APER
3, 4	MAG_APER, MAGERR_APER
5	FLUX_MAX
6, 7	*ISO*AREA_IMAGE, *ISO*AREAF_IMAGE
8–13	X2_IMAGE, Y2_IMAGE, XY_IMAGE, ERRX2_IMAGE, ERRY2_IMAGE, ERRXY_IMAGE
14–19	CXX_IMAGE, CYY_IMAGE, CXY_IMAGE, ERRCXX_IMAGE, ERRCYY_IMAGE, ERRCXY_IMAGE
20–25	A_IMAGE, B_IMAGE, THETA_IMAGE, ERRA_IMAGE, ERRB_IMAGE, ERRTHETA_IMAGE
26–33	*ISO*0, *ISO*1, *ISO*2, *ISO*3, *ISO*4, *ISO*5, *ISO*6, *ISO*7
34	FLAGS
34	FWHM_IMAGE
36	ELONGATION
37	ELLIPTICITY
38	POLAR_IMAGE
39, 40	VIGNET, VIGNET_SHIFT
41	FLUX_GROWTHSTEP
42, 43	MAG_GROWTH, MAG_GROWTHSTEP
44	FLUX_RADIUS

3.3 Difference imaging analysis

To determine the presence of transients on our surveyed fields, we conducted a difference image analysis (DIA) on them. DIA is a set of methods to perform a photometric comparison among two images of the same portion of the sky. The idea is to use a reference image that represents the 'static sky' and subtract it from the images of interest, revealing a flux excess as a result of the subtraction. This flux excess can be related to a new source, or a variable source. DIA has been applied successfully in many transient searches, e.g. the Palomar Transient Factory (PTF; Masci et al. 2017), the Nearby Supernova Factory (SNFactory; Wood-Vasey et al. 2004), Pan-STARRS (Chambers et al. 2016), and others.

When comparing images taken at different times, one of the main sources of image mismatch is the point spread function (PSF) difference between the images. There are several different approaches in the literature to deal with this issue, most notably Alard & Lupton (1998), Bramich (2008), and more recently Zackay, Ofek & Gal-Yam (2016). What all these methods have in common is the modelling of a convolution kernel that minimizes spurious residuals due to differences in instrumentation and atmospheric conditions of each observation, while at the same time unveils the flux variation of true astrophysical sources.

But even after this convolution fit, alignment deformation defects and subtle space PSF variability leave behind a large amount of spurious sources that arise only from the DIA process. Dealing with such spurious (or bogus) sources is typically done with trained machine learning (ML) classifiers, and the final veto is left to humans by visual inspection. We discuss this topic further in Section 3.4.

For our analysis, we implement the method described in Bramich (2008), which fits the convolution kernel pixels independently, to minimize the ℓ_2 norm of the subtraction image.

3.4 Real/bogus classification and detection of potential transients

As mentioned before, object detection programs usually pick many DIA artefacts as potential sources. Real transients are commonly outnumbered by these artefacts by a 1:100 ratio or even more. Given the large number of these bogus sources, it becomes necessary to train automatic ML agents to quickly identify the real transients among all the potential candidates and set them apart from bogus sources.

ML classifiers must be trained with a large number of examples of each class in order to adequately sample the feature space. Our subtraction images provide us with a large and assorted sample of subtraction artefacts (bogus) but we do not have as many examples of real transients, due to the rare nature of these events.

To compensate for the lack of real transients and to complete a balanced set for them, we injected synthetic stars on each of the science images, reusing them many times, to achieve equal number of bogus and simulated transients to improve the statistics. The injected sources were modelled after a PSF estimation of the image done by the *properimage* PYTHON package (Sánchez et al. 2018), based on a Karhunen–Loëve transform of selected stars. The magnitude distribution of the injected sources follows the distribution of the ones on the images, as detected by the SEP package (Barbary 2016).

The object detection on the subtraction images was done by the program SEXTRACTOR v2.19.5 (Bertin & Arnouts 1996), for objects with a detection significance over 3.0σ and with more than five connected pixels. A reduced set of morphological parameters given by this program was later used as input features to train different ML algorithms.

After recovering the SEXTRACTOR parameters of the injected sources, we were able to create a labelled (real/bogus) training and validation set with 2414 examples of bogus subtraction artefacts and 2439 examples of injected transients (4853 examples in total). The complete list of features used is given in Table 1.

We trained and compared a few classical ML algorithms with the generated training sets. The best performance was achieved with a random forest (RF) algorithm utilizing 10 decision trees to avoid overfitting. Boosted decision trees performed comparably to RF. The last tested algorithm was support vector machines (SVMs), with very low scores at the 60 per cent level or below. The final scores are shown in Table 2 and on Figure 1. Of all of the above, we chose the RF classifier to use in the selection of optical transient (OT) candidates.

By the end of O2, we also tried a convolutional neural network (CNN) approach. The implementation of this method is still work in progress and will not be used for production until further testing, but we describe preliminary results in Section 3.5.

Table 2. Machine learning scores.

	Random forest	Boosted decision trees	Support vector machine
Accuracy	0.89	0.89	0.65
Precision	0.92	0.91	0.79
Recall	0.86	0.87	0.48
F1-measure	0.89	0.89	0.59

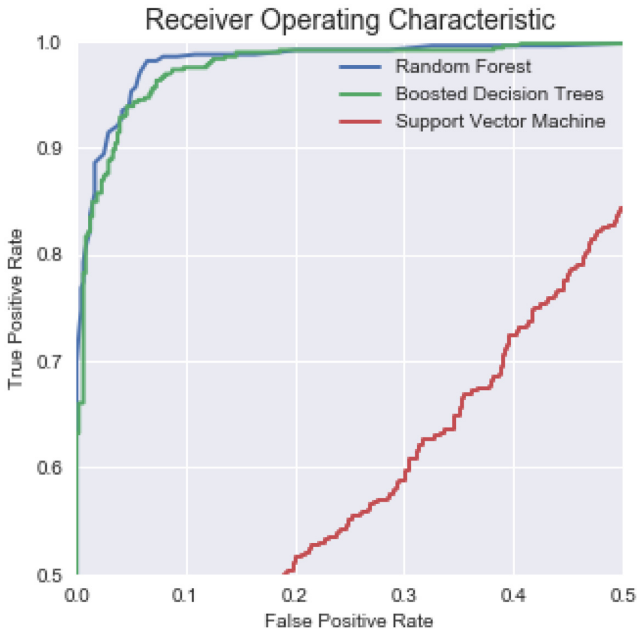

Figure 1. The receiver operating characteristic curve for our random forest, boosted decision trees, and support vector machine classifiers.

3.5 Testing convolutional neural network

Although our results show the RF method as the optimal method to find OTs in taken images, we still investigated more possible efficient methods. In this section, we describe our experimental real/bogus classification method for image subtraction based on CNNs. In general, CNN-based methods are used in image processing, and the construction of the network is inspired by real organism vision systems. The classification of real/bogus events is also an image processing problem. The method works in a similar manner as the RF algorithm on subtracted images, searching for potential OTs that might come up during the subtraction process. But CNN handles things somehow differently: it uses as input a cropped part of the subtraction image, which contains the potential source selected by SEXTRACTOR, and not the set of parameters associated with it.

The CNN method works as follows. First, SEXTRACTOR finds all the potential sources on the subtracted image above a 3σ detection threshold. Then, a 28-by-28 pixel area around a source is cropped from the image and fed to a neural network to label it as a real transient or bogus (artefact of the subtraction process). After getting the likelihood of the potential OT belonging to one of those classes, we identify its class as the class that scored higher in the classification.

The construction layers of the network are described in Table 3. We trained and tested a CNN in the same manner as we did for the RF (see Section 3.4), except that the inputs to the CNN are now the raw pixels of the cropped images, as opposed to the SEXTRACTOR parameters in the RF case. Our network achieved a 99.5 per cent accuracy on testing and training sets, matching all of the cases.[1]

To build our neural network, we used the KERAS package with a Theano backend. We chose a sequential-type model with `categorical_crossentropy` loss metric. We used the 'Adam' optimizer and accuracy metrics.

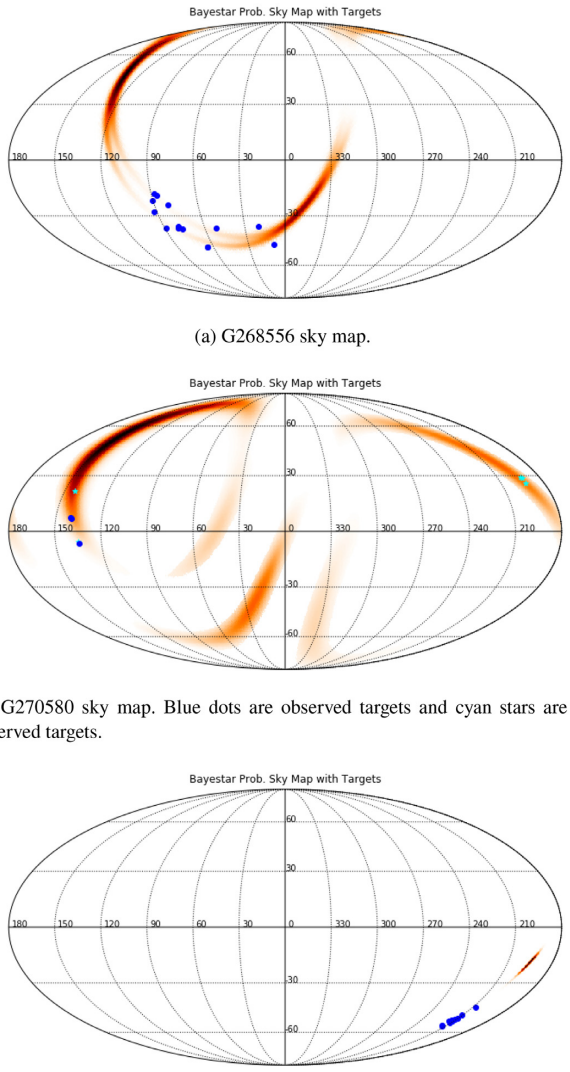

(a) G268556 sky map.

(b) G270580 sky map. Blue dots are observed targets and cyan stars are not observed targets.

(c) G298048 sky map.

Figure 2. Bayestar probability all-sky maps for the three alerts G268556, G270580, and G298048. The assigned targets are marked in blue dots.

[1] If the dropout layer between two dense layers has the parameter set to 0.6, it is possible to achieve 100 per cent accuracy.

Table 3. Construction of experimental convolutional neural network used for real/bogus classification.

Layer name	Parameters
Convolution2D	(32, 3, 3, activation='relu', input_shape=(1,21,21))
Convolution2D	(32, 3, 3, activation='relu')
MaxPooling2D	(pool_size=(2,2))
Dropout	(0.25)
Flatten	( )
Dense	(128, activation='relu')
Dropout	(0.57)
Dense	(2, activation='softmax')

Our construction of the network is a bit different from other networks like that of Cabrera-Vives et al. (2017) and Gieseke et al. (2017). In our approach, we stacked two Conv2D layers together and used high dropout values at the dense part of the network. It is important to note that our experimental solution offers better accuracy than Cabrera-Vives et al. (2017) or Gieseke et al. (2017). Our method based on CNNs will be subject to future development and will be expanded in a separate report.

4 RESULTS

4.1 G268556 (GW170104)

Once we received the GCN notice for alert G268556, the real-time system for target generation described in Section 3.1 generated a list of 35 targets. Due to weather conditions and time availability at the telescope, we observed a subset of 15 of those targets that we present in Table 4. Fig. 2(a) shows the observed targets on an all-sky Bayestar probability map.

The 15 targets correspond to 14 images, each one a combination of several individual frames. The images were taken with the EABA 1.54-m telescope, on several nights between 2017 January 13 and 21. Despite the images being taken with no filter, we estimate field depth by fitting a colour–colour diagram of the stars on the field, to find the image zero-point. The fit yields limiting magnitudes equivalent to the range 18.72–21.1 in the GSC 2.3 POSS-II *R* band. The original targets were revisited again to obtain references for image subtraction, during 2017 March and eventually, due to frosting condensation problems on the CCD, again on 2017 November.

The images were pre-processed and then analysed with the methods described in Section 3. As explained there, we used a DIA with a delta basis. Running SEXTRACTOR on it, we yielded 2375 potential sources. Most of these were subtraction artefacts that were sifted through using an RF ML agent trained as explained in Section 3.4. From the final sifting, 39 candidates remained that were human inspected individually. The visual inspection rejected them all since they were either misclassified bogus or were not persistent across individual frames.

We conclude that there were no bona fide candidates for EM transients present near to any galaxy that we have observed. It has to be pointed out that this is consistent with the current state of knowledge, where BBH mergers are not likely to produce an EM counterpart.

4.2 G270580

For alert G270580, issued on 2017 January 20, we targeted three galaxies out of eight generated by the target selection system, with a Meade LX200 16-in. telescope equipped with an SBIG STF 8300, located in Tolar Grande, Argentina.

Unfortunately, the observation conditions for the site in Salta, Argentina, where the images were taken, made the quality of the images too poor for any reasonable analysis. We, nevertheless, provide the complete list of the generated targets in Table 5. The generated targets are shown over the sky localization map in Fig. 2(b).

4.3 G298048 (GW170817)

For the alert G298048 that was later classified as the BNS merger GW170817, we ran the galaxy selection pipeline on the Bayestar probability map and generated 20 likely galaxy hosts according to the sky probability assigned by LIGO.

During the first local night, we visited 12 of those targets in six pointings, with the T80S telescope in Cerro Tololo, Chile (Díaz et al. 2017a). Other targets were visited as well with the telescope in Cordoba, Argentina, but the images were too bad to be used (Díaz et al. 2017b). The targets visited during the first night are listed in Table 6. The targets are shown over the localization map on Fig. 2(c).

When the next day a promising candidate counterpart was announced by the 1M2H Collaboration (GCN 21529), identified near NGC 4993, we ended our follow-up search and focused instead on imaging the kilonova candidate. The result of those observations is explained in more detail in Díaz et al. (2017); here, we provide a very brief summary.

On the night of August 18, we imaged the transient with the T80S facility. We took 16, 15, and 15 1-min exposures through SDSS *g*, *r*, and *i* filters, respectively, over a course of 80 min. The light curve of the said exposures exhibited a significant decline across all bands during the ∼80 min of observations.

On August 19, observations were continued using the 1.54-m telescope located at the EABA. The observations taken with EABA were done without using any astronomical filter. However, the extrapolation of values of brightness in *r* filter that we obtained is consistent with the decline trend.

The image analysis of what is now known as the AT 2017gfo kilonova departed from the detection pipeline method explained in Section 3. Since the candidate was quickly identified by another collaboration, we did not run a DIA or ML classifiers on our images. Instead, we carried out time-series PSF photometry using DAOPHOT/ALLSTAR (Stetson 1987), ALLFRAME (Stetson 1994), and related programs, kindly provided by P. Stetson, and the method outlined in Macri et al. (2006) and Macri et al. (2015).

4.3.1 Remarks about strategy and data analysis

The event GW170817 makes us reconsider the targeting strategy for future events. Our first approach for galaxy targeting used very restrictive cuts on absolute and apparent blue magnitude of the galaxy (<-17.5 and <19.0, respectively), distance (<80 Mpc), and relative position to the Sun that the object would have a zenith distance of 45 deg or lower. A list after those cuts is sorted based on its position likelihood given by LIGO's sky map, and the top 20 galaxies are considered.

NGC 4993 did not make it to that list on the first night since it was never 45 deg above the horizon for any of our observatories. Had not there been cuts on zenithal distance, NGC 4993 would have ranked 25th.

Table 4. Targeted host galaxies for G268556 (GW170104).

Date[a]	ID[b]	RA (hh:mm:ss)	Dec. (d:mm:ss)	Total t_{exp}	Distance (Mpc)	Field depth[c] R
2017-01-13	PGC 073926	01:20:36.56	−36:05:34.40	41 min	79.03	20.95 ± 0.04
2017-01-13	NGC 1341	03:27:58.39	−37:09:00.22	51 min	19.86	20.95 ± 0.04
2017-01-13	NGC 1808	05:07:42.31	−37:30:46.66	1 h 7 min	12.30	20.95 ± 0.04
2017-01-13	ESO 487-003	05:21:50.69	−23:57:04.79	6 min	51.57	20.95 ± 0.04
2017-01-13	ESO 364-014	05:55:01.31	−36:56:49.38	49 min 30 s	79.22	20.95 ± 0.04
2017-01-14	NGC 1341	03:27:58.39	−37:09:00.22	5 min	19.86	19.72 ± 0.05
2017-01-14	ESO 202-009	04:21:03.64	−48:18:14.87	47 min 25 s	61.29	19.72 ± 0.05
2017-01-14	PGC 147285	05:16:47.93	−36:04:07.79	22 min	58.22	19.72 ± 0.05
2017-01-15	ESO 242-018	00:37:06.17	−46:38:38.83	50 min	48.3	21.10 ± 0.06
2017-01-15	NGC 1567	04:21:08.75	−48:15:17.39	50 min	60.72	21.10 ± 0.06
2017-01-15	ESO 425-010	06:08:57.37	−27:48:07.45	44 min	36.32	21.10 ± 0.06
2017-01-15	PGC 3080859	05:19:35.94	−36:49:02.50	46 min	61.86	21.10 ± 0.06
2017-01-15	IC 2143	05:46:52.64	−18:43:34.82	45 min	38.02	21.10 ± 0.06
2017-01-15	ESO 555-005	05:51:39.85	−18:01:21.90	44 min 30 s	39.99	21.10 ± 0.06
2017-01-15	ESO 555-022	06:01:08.00	−21:44:19.28	42 min	20.80	21.10 ± 0.06

[a]Local date of observation.
[b]From White et al. (2011).
[c]Field depth is for an equivalent magnitude in the GSC 2.3 POSS-II *R* band. Images taken with the EABA 1.54-m telescope with an unfiltered camera.

Table 5. List of potential host galaxies for G270580.

Date[a]	ID[b]	RA (hh:mm:ss)	Dec. (d:mm:ss)	Total t_{exp}	Distance (Mpc)	Field depth[c] R
2017-01-20	PGC 1312883	09:20:01.68	07:03:22	1 h	50.16	18.30 ± 0.01
2017-01-20	UGC 04959	09:20:32.20	07:04:27	1 h	93.75	18.30 ± 0.01
2017-01-20	PGC 025197	08:58:12.00	− 06:11:57	1 h 1 min 30 s	71.75	19.67 ± 0.03
Not observed	NGC 4738	12:51:08.89	28:47:17	–	58.83	–
Not observed	NGC 2903	09:32:10.08	21:30:05	–	10.93	–
Not observed	NGC 4793	12:54:40.79	28:56:17	–	35.29	–
Not observed	NGC 4747	12:51:45.83	25:46:32	–	16.47	–
Not observed	PGC 1042309	09:00:15.11	− 05:37:49	–	65.70	–

[a]Local date of observation.
[b]From White et al. (2011).
[c]Field depth is for an equivalent magnitude in the GSC 2.3 POSS II *R* band. Images taken with Meade LX200 16-in. unfiltered camera.

Table 6. Targeted host galaxies for G298048 (GW170817).

Date[a]	ID[b]	RA (hh:mm:ss)	Dec. (d:mm:ss)	Total t_{exp}	Distance (Mpc)	Field depth[c] R	Tile #
2017-80-17	PGC 485499	14:03:11.90	− 48:37:39	14.5 min	36.54	20.21 ± 0.11	1, 5
2017-08-17	ESO175-002	14:08:36.00	− 53:21:10.00	26.5 min	59.67	20.46 ± 0.12	2, 4, 6
2017-08-17	ESO 221-030	14:10:41.12	− 52:11:02.90	22.5 min	42.32	20.63 ± 0.27	2, 6
2017-08-17	ESO221-035	14:16:04.47	− 52:36:31.00	22.5 min	51.35	20.63 ± 0.27	2, 6
2017-08-17	PGC 141857	14:10:33.49	− 52:19:01.42	22.5 min	41.72	20.63 ± 0.27	2, 6
2017-08-17	PGC 448694	14:10:37.02	− 52:06:05.90	22.5 min	56.19	20.63 ± 0.27	2, 6
2017-08-17	ESO271-003	13:52:27.36	− 43:52:52.00	16 min	20.69	20.63 ± 0.27	2
2017-08-17	ESO221-028	14:09:02.15	− 51:10:07.00	4 min	62.47	20.18 ± 0.12	3
2017-08-17	PGC 463082	14:03:29.27	− 50:46:37.60	4 min	45.79	20.18 ± 0.12	3
2017-08-17	PGC 166323	14:04:34.10	− 52:41:49.99	4 min	49.42	19.81 ± 0.25	4
2017-08-17	PGC 141859	14:20:23.53	− 55:04:06.64	9 min	36.67	19.95 ± 0.08	5
2017-08-17	PGC 2800412	14:17:10.00	− 55:37:11.64	9 min	52.58	19.95 ± 0.08	5

[a]Local date of observation.
[b]From White et al. (2011).
[c]Field depth is for an equivalent 5σ magnitude in the GSC 2.3 POSS II *R* band. Images taken with T80S 0.826-m in Sloan *r* filters.

From this experience, we revise our strategy for choosing targets. First of all, cuts rejecting galaxies must not be too conservative, they should be as low as possible giving a chance for operators and AI systems at the observatories to reject galaxies that fall below the horizon. Secondly, from event GW170817, we can assume with high probability that OTs connected with a kilonova will occur next

to massive galaxies. In the area of the LIGO final sky map where probability was higher than 10^{-6} per sky map's pixel, NGC 4993 was the sixth most massive galaxy.

We checked a few different strategies for choosing target galaxies that will be implemented in LIGO's O3 science run. The best strategy consists of following a ranking statistics along with a product of the likelihood and the absolute magnitude of the galaxy. In this ranking statistics, NGC 4993 comes in sixth place. Galaxies are only rejected based on the possibility of observation from the current location; the cut-off position above the horizon is based on requests from the given observatory. This strategy will be subject to future testing during the O3 science run.

Another related improvement comes from the use of more complete catalogues. During O2, we relied on the GWGC catalogue (White et al. 2011), which contains objects no farther than 100 Mpc. The GLADE catalogue (Dálya et al. 2018) extends the reach of the GWGC catalogue by several hundreds of Mpc. The GLADE catalogue is still ∼40 per cent complete even up to distances as far as 200 Mpc. For O3, we plan to have the GWGC catalogue replaced in all of our response systems.

5 THE TOROS OBSERVATORY AT CORDÓN MACÓN

To participate in the upcoming O3 LIGO VIRGO observational campaign, we are currently installing a system with a primary mirror diameter of 0.6 m, which will in its final design stage have a large field-of-view (10 deg^2) camera with a very broad bandpass (0.4–0.9 μm, equivalent to a combination of the Sloan *griz* filters). The system will be installed atop Cordón Macón located in the Atacama portion of Northwestern Argentina. This dedicated instrument to follow up GW candidate events in the Southern hemisphere will fill a niche and offer extended coverage of the southern skies. The telescope (Planewave CDK24 with LT500 mount) and its dome (Ashdome Lanphier type) are currently undergoing installation at the site. We plan to equip the telescope with a 10 K × 10 K backside-illuminated STA1600LN CCD and prime-focus corrector to maximize the field of view of the telescope. It is worth noting that even in below average conditions, TOROS remains sensitive (SNR > 3) to kilonova events like AT 2017gfo for at least 4 d.

6 SUMMARY

The TOROS Collaboration conducted a prompt search for EM counterparts to GW events reported by the LIGO–Virgo detectors during their second science run (O2) using several instruments in different facilities distributed over Argentina, Chile, and United States. The quality of some of the data was not suitable for analysis, but we successfully processed data from the 1.5-m telescope of EABA in Córdoba, Argentina and the T80S at the Cerro Tololo Inter-American Observatory, Chile.

We responded to three LIGO alerts: GW170104, a BBH merger; G270580, a retracted false alarm; GW170817, a BNS merger. For GW170104, we performed detailed analyses to search for optical counterparts associated with the GW event. We did not find any optical counterpart to GW170104, an expected result for an event classified as a BBH merger. For GW170817, once the optical counterpart candidate AT 2017gfo (SSS17a) was discovered by the 1M2H Collaboration (GCN 21529), we obtained images of the optical counterpart and produced light curves in SDSS *g*, *r*, and *i* bandpasses. The data gathered by the TOROS Collaboration were part of the important worldwide observations of the first joint GW–EM observation. It was also the first kilonova associated with a GW ever observed.

The discovery of the optical counterpart to GW170817 in close proximity to NGC 4993 proves that the strategy used to identify EM counterparts to GW transient is appropriate. The strategy, a galaxy-based approach, focuses the search on the most massive galaxies in the probability area of origin of the GW.

The TOROS network is expanding, and for the O3 LIGO–Virgo science run, we expect to have two fully dedicated sites for fast transient search: one in Salta, Argentina and one in Brownsville, Texas. Both the observatories will be fully robotic. In addition, the collaboration has strengthened their capabilities by observation time allocated at the Gran Telescopio de Canarias (20-MULTIPLE-3-19AMEX; PI: Omar López-Cruz), Gemini South (GS-2019A-Q-122; PI: Diego G. Lambas), and the FALCON Telescope Network (Chun et al. 2018) (FTN-MMO-20180010; PI: Nilo Castellon).

ACKNOWLEDGEMENTS

The TOROS Collaboration acknowledges support from Ministerio de Ciencia, Tecnología e Innovación Productiva (MINCyT) and Consejo Nacional de Investigaciones Científicas y Tecnológicas (CONICET) from Argentina, grants from the National Science Foundation of the United States of America, NSF PHYS 1156600 and NSF HRD 1242090, and the government of Salta province in Argentina. The T80-South robotic telescope (Mendes de Oliveira et al., submitted) was founded as a partnership between the São Paulo Research Foundation (FAPESP, grant number 2009/54202-8), the Observatório Nacional (ON), the Federal University of Sergipe (UFS), and the Federal University of Santa Catarina (UFSC), with important financial and practical contributions from other collaborating institutes in Brazil, Chile (Universidad de La Serena), and Spain (CEFCA). JLNC is grateful for financial support received from the GRANT PROGRAMMES FA9550-15-1-0167 and FA9550-18-1-0018 of the Southern Office of Aerospace Research and Development (SOARD), a branch of the Air Force Office of the Scientific Research International Office of the United States (AFOSR/IO). NCNR is grateful for financial support from MNiSW grant DIR/WK/2018/12 and NCN grant UMO-2017/26/M/ST9/00978.

Facilities: EABA, T80-S, and TORITOS.

REFERENCES

Abbott B. P. et al., 2016a, Living Rev. Relativ., 21, 3
Abbott B. P. et al., 2017, ApJ, 848, L12
Acernese F. et al., 2015, Class. Quantum Gravity, 32, 024001
Alard C., Lupton R. H., 1998, ApJ, 503, 325
Barbary K., 2016, J. Open Source Softw., 1, 58,
Barnes J., Kasen D., 2013, ApJ, 775, 18
Benacquista M. et al., 2014, in Walton N. A., Figueras F., Balaguer-Nunez L., Sourbiran C., eds, The Milky Way Unravelled by Gaia: GREAT Science from the Gaia Data Release, Vol. 67. EAS Publication Series, EDP Science, Paris, France, p. 357
Berger E., 2014, ARA&A, 52, 43
Bertin E., Arnouts S., 1996, A&AS, 117, 393
Bramich D. M., 2008, MNRAS, 386, L77
Cabrera-Vives G. et al., 2017, ApJ, 836, 97
Chambers K. C. et al., 2016, preprint (arXiv:1612.05560)
Chun F. K. et al., 2018, PASP, 130, 095003
Cowperthwaite P. S., Berger E., 2015, ApJ, 814, 25
Dálya G. et al., 2018, MNRAS, 479, 2

Díaz M. C. et al., 2017, ApJ, 848, L29
Díaz M. C. et al., 2017a, GCN Circ., 21619
Díaz M. C. et al., 2017b, GCN Circ., 21620
Gieseke F. et al., 2017, MNRAS, 472, 3
Hanna C., Mandel I., Vousden W., 2014, ApJ, 784, 8
Lang D. et al., 2010, AJ, 139, 1782
Li L.-X., Paczyński B., 1998, ApJ, 507, L59
LIGO Scientific Collaboration, 2015, Class. Quantum Gravity, 32, 074001
LIGO Scientific Collaboration, Virgo Collaboration, 2017a, GCN Circ., 20364
LIGO Scientific Collaboration, Virgo Collaboration, 2017b, GCN Circ., 20486
LIGO Scientific Collaboration, Virgo Collaboration, 2017c, GCN Circ., 21509
LIGO Scientific Collaboration, Virgo Collaboration, 2018, Phys. Rev. X, 9, 031040
Macri L. M., Stanek K. Z., Bersier D., Greenhill L. J., Reid M. J., 2006, ApJ, 652, 1133
Macri L. M., Ngeow C.-C., Kanbur S. M., Mahzooni S., Smitka M. T., 2015, AJ, 149, 117
Masci F. J. et al., 2017, PASP, 129, 014002
Metzger B. D., Berger E., 2012, ApJ, 746, 48
Nakar E., Piran T., 2011, Nature, 478, 82
Renzi V. et al., 2009, Bol. Asociacion Argentina Astron. Plata Argentina, 52, 285
Sánchez B. et al., 2019, Astronomy and Computing, 28, 100284
Stetson P. B., 1987, PASP, 99, 191
Stetson P. B., 1994, PASP, 106, 250
Tremblin P., Schneider N., Minier V., Durand G. A., Urban J., 2012, A&A, 548, A65
White D. J., Daw E. J., Dhillon V. S., 2011, Class. Quantum Gravity, 28, 085016
Wood-Vasey M. N. et al., 2004, New Astron. Rev., 48, 637
Zackay B. et al., 2016, ApJ, 830, 27

[1]*Universidad Nacional de Córdoba, IATE, Córdoba, Argentina*
[2]*Center for Gravitational Wave Astronomy, The University of Texas Rio Grande Valley, Brownsville, 78500 TX, USA*
[3]*Instituto Nacional de Astrofísica, Óptica y Electrónica, Tonantzintla, Puebla, México*
[4]*Departamento de Astronomía, Universidad de La Serena, La Serena, 1720236, Chile*
[5]*George P. and Cynthia W. Mitchell Institute for Fundamental Physics and Astronomy, Department of Physics and Astronomy, Texas A&M University, College Station, 77845 TX, USA*
[6]*Instituto de Astronomía, Universidad Nacional Autónoma de México, AP 70-264, 04510 México D.F., Mexico*
[7]*Instituto de Astrofísica, Pontificia Universidad Católica de Chile, Santiago, 8970117, Chile*
[8]*Universidade Federal de Santa Catarina, Florianópolis, 88040-900, Brazil*
[9]*Instituto de Investigación Multidisciplinario en Ciencia y Tecnología, Universidad de La Serena, La Serena, 1720468, Chile*
[10]*Large Synoptic Survey Telescope, Tuscon, 85719 AZ, USA*
[11]*Department of Physics, Duke University, Science Dr, Durham, NC 27710, USA*
[12]*Universidade Federal do Rio Grande do Sul, Porto Alegre, 90040-060, Brazil*
[13]*National Centre for Nuclear Research, Astrophysics Division, ul. Pasteura 7, PL 02-093 Warsaw, Poland*

This paper has been typeset from a TEX/LATEX file prepared by the author.